Journal of Alloys and Compounds 504 (2010) 519–526

Contents lists available at ScienceDirect

Journal of Alloys and Compounds

journal homepage: www.elsevier.com/locate/jallcom

Influence of sodium silicate concentration on structural and tribological properties of microarc oxidation coatings on 2017A aluminum alloy substrate

Aytekin Polat[a,*], Murat Makaraci[b], Metin Usta[c]

[a] Department of Mechanical Engineering, Nigde University, Nigde 51100, Turkey
[b] Department of Mechanical Engineering, Kocaeli University, Kocaeli, Turkey
[c] Department of Materials Science and Engineering, Gebze Institute of Technology, Kocaeli, Turkey

ARTICLE INFO

Article history:
Received 2 March 2010
Received in revised form 21 May 2010
Accepted 1 June 2010
Available online 11 June 2010

Keywords:
Alumina coating
Microarc oxidation
Surface roughness
Adhesion
Wear

ABSTRACT

In this paper, thick and hard oxide coatings resistant to wear were produced on 2017A–T6 Al alloy by the microarc oxidation (MAO) technique in an alkali electrolyte consisting of different sodium silicate concentrations (0–8 g/l). The coatings were characterized by means of optical microscopy, scanning electron microscopy (SEM), X-ray diffraction (XRD) and surface profilometry. Microhardness, scratch adhesion and pin-on-disk sliding wear tests were also performed to evaluate the tribological properties of the coatings. The influence of sodium silicate concentration on the structural and tribological properties of the MAO coatings was discussed. Results reveal that increasing sodium silicate concentration from 0 to 8 g/l in the electrolyte caused an increase in the electrolyte conductivity (from 7.71 to 18.1 mS/cm) and a decrease in positive final voltage (from 627 to 590 V) in the MAO process. In response to the increase in sodium silicate concentration, the thickness, surface roughness (R_a) and critical load (L_c) corresponding to adhesive failure of the coatings were increased simultaneously from 74 to 144 μm, and 4.4 to 6.58 μm, and 127.76 to 198.54 N, respectively. At the same time, the phase structure and composition of the coatings also varied by the participation of silicate ions in the reactions and their incorporation into the coating structure. Moreover, it was observed that the coating formed in the low sodium silicate concentration (4 g/l) had higher surface hardness (2020 HV) and improved wear resistance than the one (1800 HV) formed in the high sodium silicate concentration (8 g/l). The coatings produced in three different electrolytic solutions provided an excellent wear resistance and a load carrying capacity compared to the uncoated aluminum alloy.

1. Introduction

Aluminum, one of the most weight-saving materials and the second most existing metal in the earth, shows much superior performance than the conventional materials due to its high strength to density ratio and easy formability. However, aluminum alloys have low hardness, poor tribological properties and relatively low yield strength when compared with steels and cast-irons. As a result, these materials are vulnerable to wear in sliding and rolling contact situations [1]. The way of avoiding the wear formation both on high strength and low strength metals is to modify their surfaces to resist wear. There are many known ways of performing this. One of them is to change the surface modification of metals by depositing oxide-resulting elements to the surfaces. The other one is to change the structure of the surfaces by heat treatment or by adding new alloying elements. Related to the former, various metallic and ceramic coatings have been studied and applied by surface modification processes such as physical vapor deposition (PVD), chemical vapor deposition (CVD), ion beam assisted deposition (IBAD), hard anodizing, thermal spraying, laser surface alloying, and sol–gel [2]. However, TiN, CrN or diamond-like carbon (DLC) coated aluminum alloys by various PVD methods often exhibit limited tribological performances due to the elastic and plastic deformation of the substrate under mechanical loading, since the coatings are usually too thin to support heavy loads and protect the substrate at the contact points [3,4]. Hard anodizing and thermal spraying have suffered from the low load support of the underlying material and/or insufficient adhesion, which reduce their durability [5]. Moreover, most of the methods mentioned above involve high temperatures during processing, which may degrade the coating and/or substrate and may not be suitable for deposition of alumina coatings on relatively low-melting-point substrates, such as aluminum alloys.

* Corresponding author. Tel.: +90 388 2252481; fax: +90 388 2250112.
E-mail address: apolat@nigde.edu.tr (A. Polat).

0925-8388/$ – see front matter © 2010 Elsevier B.V. All rights reserved.
doi:10.1016/j.jallcom.2010.06.008

Table 1
MAO process parameters at different electrolyte compositions.

Solution code	Electrolyte composition	Conductivity (mS/cm)	Final voltage (V) (negative/positive)
E_1	2 g/l KOH, distilled water	7.74	143/627
E_2	4 g/l ·$Na_2SiO_3{\cdot}5H_2O$, 2 g/l KOH, distilled water	11.2	162/607
E_3	8 g/l $Na_2SiO_3{\cdot}5H_2O$, 2 g/l KOH, distilled water	18.1	178/590

A relatively novel method, called microarc oxidation (MAO) has been developed to produce thick and hard ceramic coatings on Al, Ti, Mg metals and their alloys [6–8]. The MAO technique is known by various names such as plasma electrolytic oxidation, plasma anodizing, and anodic spark deposition [9]. MAO is based on the conventional anodic oxidation of processing metals and alloys in aqueous electrolyte solutions under the additional condition of plasma discharge at exceeding the critical values of the polarization potential [10]. The process consists of numerous simultaneous plasma discharges leading to localized high temperature and high pressure over the surface of specimen [11]. This method combines the electrochemical oxidation with a high voltage spark treatment resulting in corrosion and wear resistant coatings [12]. In addition, this method is economically efficient, ecological friendly and characterized by high productivity. Moreover, bulk material temperature is kept less than 100 °C in this process.

The properties of MAO coatings are affected by the processing parameters, such as composition of electrolyte and alloy [13], electrolyte temperature, treatment time and voltage [14], and current density [15–17]. High quality coatings can be formed by suitable selection of these process parameters. From this point of view, the composition and the concentration of electrolyte during the process play a crucial role in obtaining the desired coatings of special phase component and microstructure. Significant progress have been made on the preparation of MAO coatings in various specially selected electrolytes and their combinations in order to provide protective coatings of corrosion, wear resistant and functional coatings on the Al alloys in the past decades [18–36]. Among these electrolytes, aqueous solutions of silicates, which are able to passivate the aluminum surfaces over a wide range of potentials and temperatures, were found to be some of the most suitable electrolytes for this method [18–21].

The earlier studies [22–33] mostly focused on optimization of electrolytes composition and concentration in order to obtain coatings with special phase composition. However, the systematic effects of the sodium silicate concentration on the structural and tribological properties of such coatings are not yet clear. The principal aim of the present work is to study systemically the influence of the sodium silicate concentration on the microstructure, phase structure, hardness, surface roughness, adhesion and wear properties of the oxide coatings formed on 2017A T6 alloy.

2. Experimental

Rectangular samples ($45 \times 25 \times 4\,mm^3$) of aluminum alloy Al-2017A were used as substrates; the nominal composition of this alloy by wt.% is 0.53% Si, 0.25% Fe, 4.34% Cu, 0.60% Mn, 0.76% Mg, 0.17% Zn, 0.02% Ti, 0.02 Zr and Al is the balance. Prior to the coating, samples were polished with abrasive papers up to 1200 grits, degreased with acetone and rinsed with distilled water. The MAO treatment device consisted of an alternating current power supply unit with 100 kW, a stainless steel container, a stirring and cooling system. The stainless steel container and the Al alloy samples were used as cathode and anode, respectively. To study the effect of sodium silicate concentration on the structural and tribological properties of MAO coatings, three kinds of aqueous electrolytes were prepared to produce the coatings. The electrolytes prepared from potassium hydroxide (KOH) and different concentrations of sodium silicate in distilled water denoted by E_1, E_2, and E_3.The conductivity of the electrolytes was determined by a conductivity meter (Mettler-Toledo, Germany). According to the discharge characteristics that appeared during the processes, different process final voltages were determined. During MAO processing, the electrolyte temperature was controlled to remain lower than 35 °C, by cooling the electrolyte solution with a heat exchanger situated in the electrolytic cell. The current density was predefined as $0.150\,A/cm^2$. All the samples to be coated were treated for 150 min. The electrolytes composition, electrolyte conductivity and relevant final voltages are given in Table 1.

At the end of the coating process, the power supply was switched off and samples were taken out of the electrolytic bath, washed in running water, dried with warm flowing air. The thickness of the MAO coatings was measured using an eddy-current coating thickness measurement gauge (Fisher, Germany) at 20 randomly selected locations. The surface roughness (R_a) was measured using a Veeco Dektak^6 profilometer and average values were calculated. Phases of as-deposited and polished MAO coatings were investigated by means of Rigaku X-ray diffractometer. Philips field emission SEM was employed to examine the microstructure and cross-sectional morphology of coatings. In addition, the measurement of cross-sectional microhardness was measured by an Anton Paar microhardness tester. The micro scratch mode of the Nanovea scratch test machine was adopted to assess the adhesion strength of the coating to the substrate. The test involved drawing a diamond stylus of 0.2 mm radius over the coating surface at a constant traveling speed of $5\,mm\,s^{-1}$ and at continuously increasing load. The critical load (L_c) at which adhesive failure of the coating occurred was detected by optical microscopic examination of the scratch track after the test, and was used as a measure of the coating adhesion strength. The tribological behavior of the specimens was measured by the pin-on-disc tribometer (CSM Instruments) under unlubricated condition at room temperature (RT) and in ambient atmosphere. A tungsten carbide (WC) ball of 6 mm diameter was used as counter face sliding partner against MAO coating. The tests were carried out at a normal load of 5 N for 5 km at 25 °C with a maximum sliding speed of 3 cm/s and amplitude of 18 mm. The relative humidity was between 52% and 83%. The frictional force was measured by a load cell attached to the loading arm and recorded by the computer through the data login and acquisition system. Then, the depths of wear track of coatings were measured from the wear grooves by using Veeco Dektak 8 surface profilometer.

3. Results and discussions

3.1. Morphology of the coating

Fig. 1 shows the surface morphologies of the oxide coatings deposited at different solutions. As it is seen from Fig. 1, the coating surfaces contain many randomly distributed pores with different size and shapes appearing as dark circular spots. Each pore serves as a discharge channel. The pores are surrounded by molten oxide that is rapidly solidified. The porous feature strongly depends on discharging nature involved in the MAO mechanism [7]. As the sodium silicate concentration increases, the number of such micro discharge channels on the surface decreases. It can also be seen that the pore size of the micro discharges increases. This is based on the fact that multiple discharging occurs at a relatively weak local region of the coating or several discharging channels connect and finally incorporate into a single larger channel. As a result, the pore size and porosity of the coating are increased.

The cross-sectional micrographs of MAO coatings are shown in Fig. 2(a)–(c) and reveal that MAO coatings consist of three layers: a porous outer layer (1); a dense inner layer (2); and a thin interfacial layer (3) below the dense layer. Such kind of coating structure was also reported by other researchers [1]. The porous outer layer (1) predominantly consists of low temperature phases (γ-Al_2O_3). The dense inner layer (2) is formed by high temperature modifications and consists of α-Al_2O_3 phase. The thin interfacial layer (3) consists of complex phases of the substrate alloying elements. The thickness, structure and composition of these three layers change relatively each other with the sodium silicate concentration. Increasing the sodium silicate concentration in the solution leads to increase both the thickness of the dense and porous outer layer of the coatings, simultaneously. The dense layers in the coatings produced in the solution of E_1, E_2 and E_3 have a thickness about 62, 70 and 82 μm, respectively while the outer porous layers

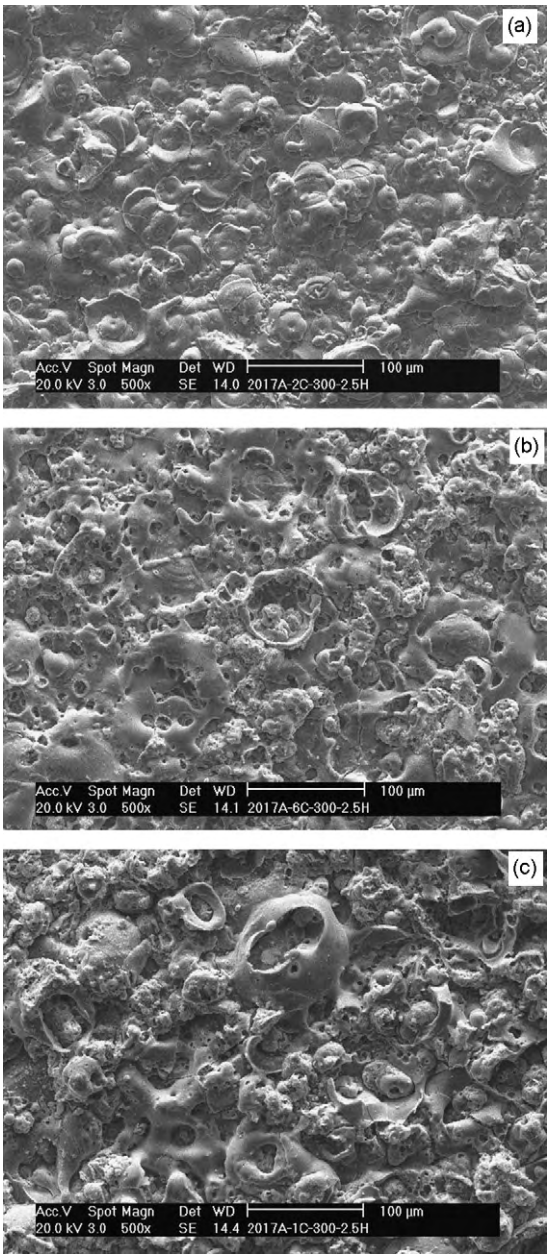

Fig. 1. Surface morphologies of oxide coatings deposited in different solutions: (a) E_1; (b) E_2; (c) E_3.

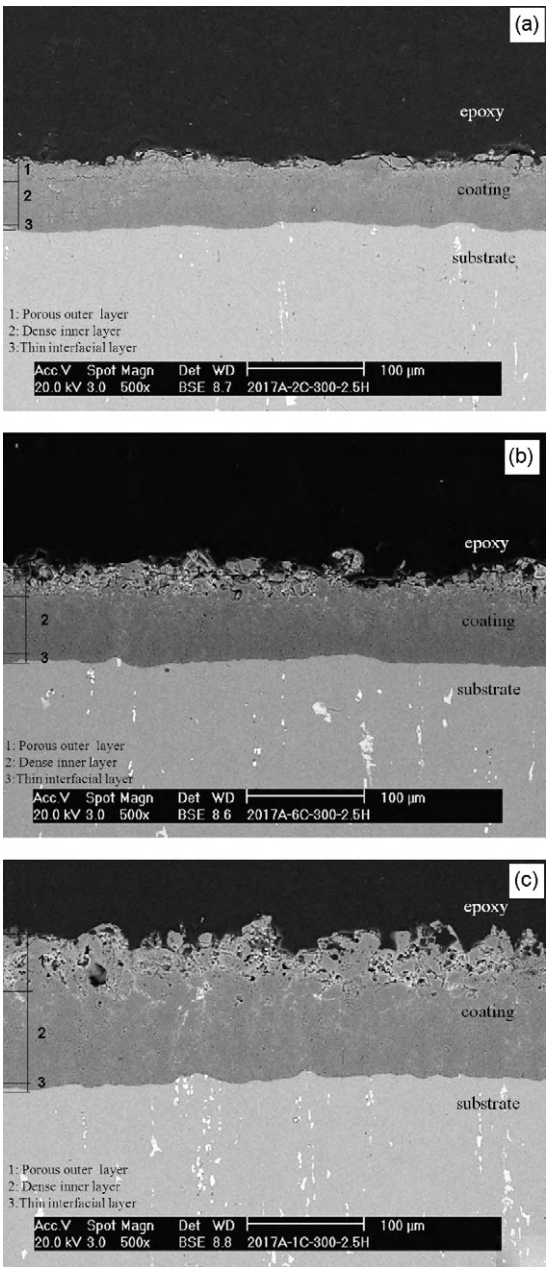

Fig. 2. Cross-section of the coatings deposited in different solutions: (a) E_1; (b) E_2; (c) E_3.

in the coatings have a thickness about 10, 22 and 30 μm, respectively. Although the thickness of the dense layer of the coating produced in the E_3 was higher than the one of the coating produced in the E_2 solution, its microstructure seems to be looser than that of the coating produced in the E_2 solution. This is based on the fact that intensive micro discharges occur and release more energy on the thick coating [9,12,25] produced in higher sodium silicate concentration and cause structural defects leading to a loose and coarse-grained structure. The dense layer shows better mechanical properties than the porous layer [9]. Therefore, a thick dense layer is favorable for the coating quality.

3.2. Presence of phases

Fig. 3 illustrates the XRD patterns of the oxide coatings deposited on Al 2017A alloy in the three electrolytic solutions. It is seen that the coating produced in E_1 solution is only composed of γ-Al_2O_3

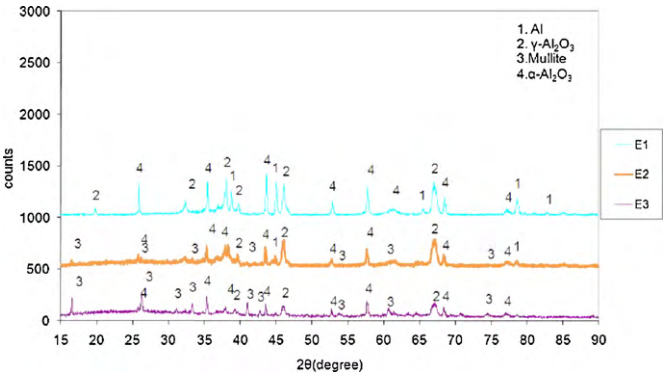

Fig. 3. XRD patterns of the oxide coatings deposited on Al 2017A alloys in the different solutions: E_1, E_2, and E_3.

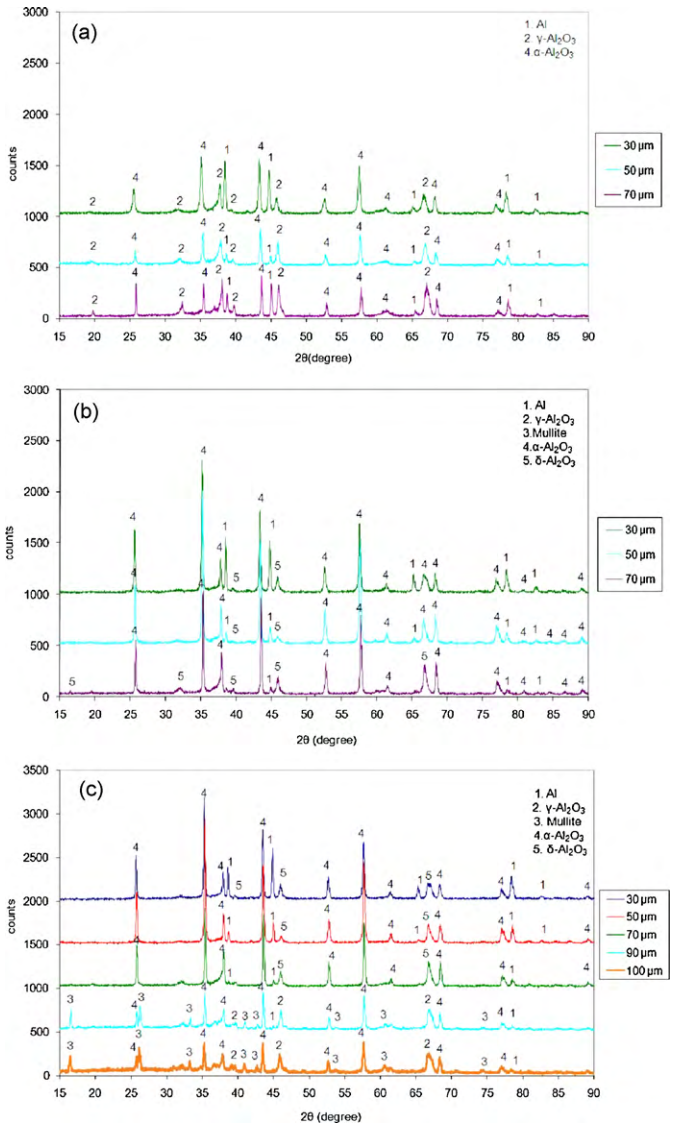

Fig. 4. XRD patterns of the inner layers at different distance from the interface of the oxide coatings deposited in the different solutions: (a) E_1; (b) E_2; (c) E_3.

and α-Al_2O_3 phases while the coatings produced in E_2, E_3 solutions are composed of γ-Al_2O_3, α-Al_2O_3 and mullite ($3Al_2O_3{\cdot}2SiO_2$) phases. The characteristic diffraction peaks of α-Al_2O_3, γ-Al_2O_3, and mullite phases in the coating produced different solutions are different. As the sodium silicate concentration in the solution increases, the intensity of diffraction peaks of α-Al_2O_3 and γ-Al_2O_3 decreases while the intensity of mullite phases increases. This is mainly caused by incorporation of silicate ions into coating structure in the form of mullite phase. The existing silicon in the form of mullite phase comes from the electrolyte constituents during the plasma chemical reaction. The mullite phase is found only in the loose outer layer of the coatings and its amount is increased by increasing the sodium silicate concentration.

The phase composition of MAO coatings depends on coating parameters and coating thickness and varies from surface to interface of coating/substrate [6,9,34]. In order to observe this variation, the coatings produced in the different solutions were grounded layer by layer many times from surface to interface of coating/substrate until a coating layer with 30 μm thickness remained on the surface of each coating. XRDs conducted on the grounded inner layers for each time are shown in Fig. 4(a)–(c). With grounding the coating layers, the content of mullite and γ-Al_2O_3 gradually

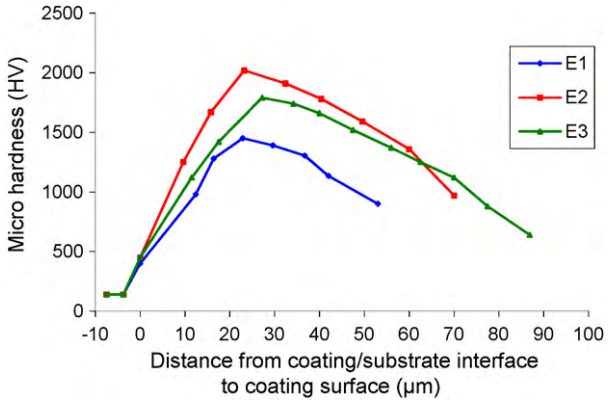

Fig. 5. Influence of the sodium silicate concentration on the hardness profile of the coating.

decreases along the coating thickness. The α-Al_2O_3 content continuously increases from surface to interface of coating/substrate. The characteristic diffraction peaks of α-Al_2O_3 phase in the coating produced in E_2 solution (Fig. 4(b)) are stronger than those in E_1 and E_3 solutions (Fig. 4(a) and (c)). This indicates that the content of α-Al_2O_3 phase in the coating produced E_2 solution is higher than those in E_1 and E_3 solutions. Further study revealed that among the coatings produced in three solutions; the content of γ-Al_2O_3 phase was the highest in the coating produced E_1 solution while the content of mullite phase was highest in the coating produced E_3 solution. Both γ-Al_2O_3 and mullite phase in E_2 and E_3 solutions disappear at about 70 μm from the interface. The main phase in the coating produced E_2 and E_3 should be α-Al_2O_3 phase, while the one in the coating produced in solution E_1 is γ-Al_2O_3 phase. The difference in the content of γ-Al_2O_3 and α-Al_2O_3 in the outer layer and internal layers of the coatings is mainly caused by variation in the cooling rate of the molten alumina in the microarc zone [6]. The porous outer layers directly connected with electrolyte solution have a higher cooling rate, which promotes the formation of γ-Al_2O_3 phase during the solidification of alumina. However, in the inner layer of the coating, the cooling rate is smaller because of the low thermal conductivity of alumina in the coating. The underlying layers of the coatings remain hotter and the temperature is high enough to transform the originally formed γ-Al_2O_3 to δ-Al_2O_3 and α-Al_2O_3.

3.3. Hardness of the coating

The cross-sectional microhardness distribution of the coatings produced in different solutions is illustrated in Fig. 5. As it is seen in Fig. 5, the microhardness distribution of MAO coatings is not

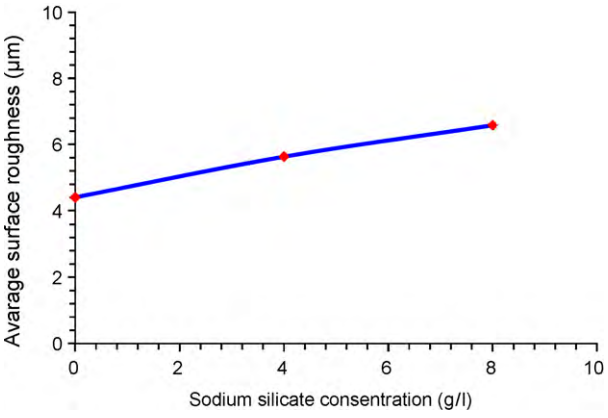

Fig. 6. Influence of the sodium silicate concentration on the surface roughness.

homogeneous. From the coating/substrate interface to the outer layer of the coating, hardness first increases with distance and reaches its maximum value. After reaching its maximum value, the microhardness of MAO coatings begin to decrease gradually towards the coating surface. Such kind of microhardness distribution was reported in [17,35]. This is attributable to both phase composition changes and a corresponding increase in the coating porosity. The ceramic coatings are mainly composed of α-Al_2O_3, γ-Al_2O_3 and mullite phases. The distribution of these phases defines the hardness profile of the coating. As it is seen in Fig. 5, the microhardness values of the coating produced in solution E_1 are less than the ones produced in the E_2, and E_3 solutions, because the coating produced in this solution is mainly consists of γ-Al_2O_3 phase with low hardness, while those produced in E_2 and E_3 are mainly composed of α-Al_2O_3 phase with high hardness. The microhardness of the coating produced in E_3 solution is relatively lower than the one produced in E_2 solution, because the layers of the coating produced in E_3 solution are less compact than that produced in E_2 solution and content of α-Al_2O_3 phase in the coating produced E_3 solution is less than that in E_2 solution. The difference in the hardness of the coating is greater especially in the outer surface of the coatings. The reason for this is that increasing the sodium silicate concentration in the electrolyte leads to accelerated coating growth and substantial increase in formation of mullite phase and coating porosity which reduces the hardness of coating. The surface microhardness (140 HV) of 2017A aluminum alloy substrate was significantly increased to the hardness of 1478 HV, 2020 HV and 1800 HV after the coatings produced in the solutions of E_1, E_2 and E_3, respectively.

3.4. Surface roughness of the coating

Fig. 6 shows the influence of the sodium silicate concentration on the surface roughness. The introduction of sodium silicate into the electrolytic solution leads to significant changes in the discharge characteristics of the sparks at the surface. High sodium silicate leads to increased sparking discharge intensity and contributes the accumulation of the coating products and forms a coarse-grained structure leading to high surface roughness. The low sodium silicate tends to form fine grain structure and causes lower surface roughness than the high sodium silicate. Furthermore, the microarc oxidation coating prepared from high sodium silicate solution has a higher total coating thickness than those prepared from low and without sodium silicate solutions. With increasing the thickness, the surface of MAO coatings is gradually roughened as a result of the reducing the pore number and as well as the increasing pore size. This observation is in good agreement with an earlier study [22]. As it is seen from Fig. 6, after 4 g/l sodium silicate concentration, the increasing trend in the surface roughness of the coating decreases slightly with increasing the sodium

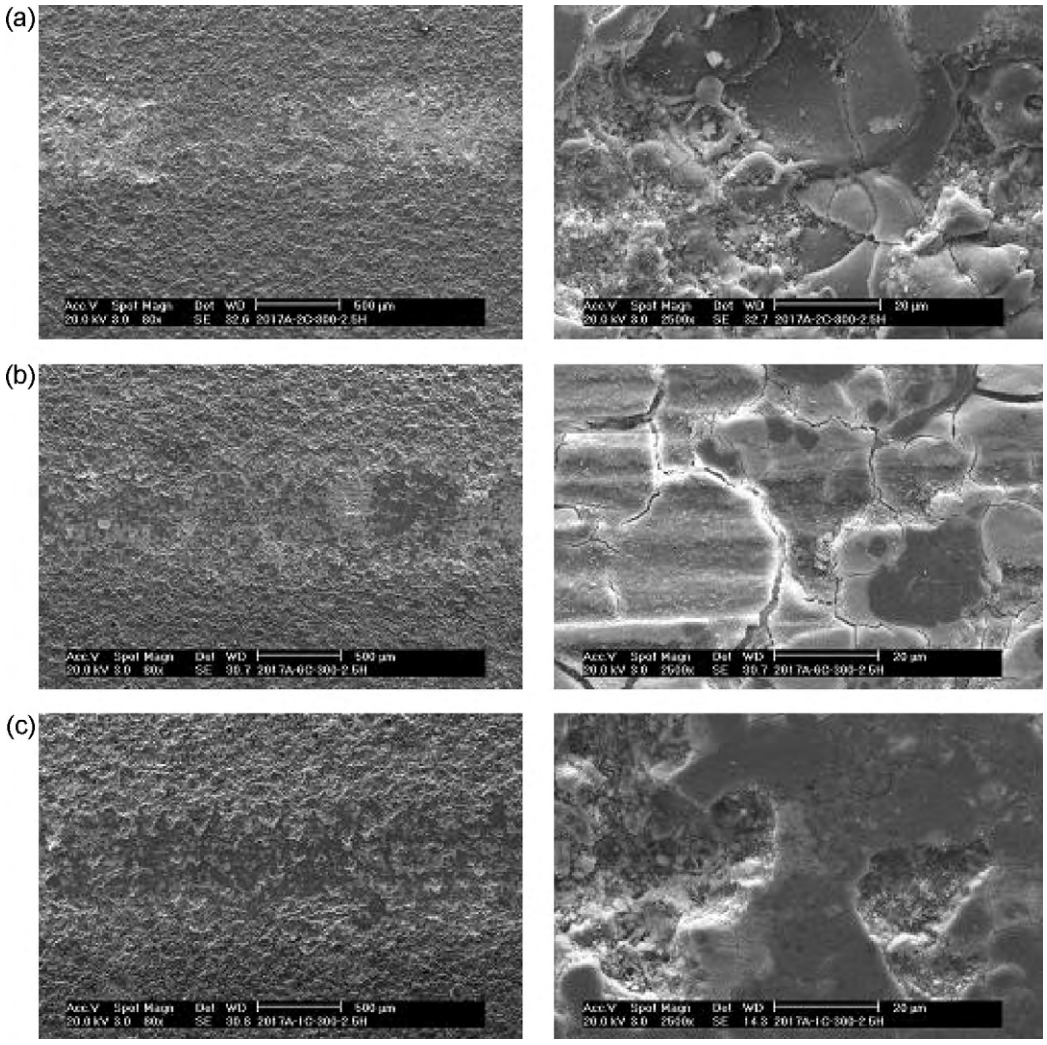

Fig. 7. SEM morphologies of wear tracks of microarc oxidation coating produced different solutions against WC ball: (a) solution E_1; (b) solution E_2; (c) solution E_3.

Table 2
Wear results of coatings produced in different solutions.

Solution	As-deposited oxide coatings		Polished oxide coatings	
	Friction coefficient	Depth of wear track of coating (μm)	Friction coefficient	Depth of wear track of coating (μm)
E_1	0.535	9.7	0.388	0.6
E_2	0.588	12.4	0.459	0.3
E_3	0.872	17.3	0.405	0.4

silicate concentration. This could be attributed to the large discharge sparks with a long time occurring on the surface of thick coating. Because the large discharge sparks release more energy and cause the coarse-grained discharge products leading to high surface roughness to melt.

3.5. Tribological properties of the coating

SEM morphologies of the sliding wear tracks with magnifications of 80× (left) and 2500× (right) of microarc oxidation coatings produced in different electrolytic solutions tested against a tungsten carbide (WC) ball at 5 N load are shown in Fig. 7. After the investigation of the surface morphology of the coatings exposed to wear, the type of wear mechanism was identified as an abrasive wear. As it is seen from SEM images of the coatings produced in different solutions, there are differences in the wear tracks morphologies of the coatings worn off. The surface of the coating produced in the solution (E_1) without sodium silicate was not worn off in a homogeneous way while the ones produced in the solution (E_2) and (E_3) were worn off in a homogeneous way and were flattened. Some cracks were detected on the surfaces of the coatings. Coating damage occurred on the regions surrounded by the cracks on the loose outer layer of the coating produced in the solution E_3. No coating delamination has been observed in the oxidized specimens throughout the test.

3.6. Friction coefficient

The results of the average friction coefficient of coatings produced different solutions derived from the pin-on-disc sliding wear tests are given in Fig. 8. All the three curves show that the friction coefficients are low at the beginning, then gradually increase and then remain constant with distance. The trend of the initial "run-in" stage of wear test is due to the surface structure and roughness. Because the outer surface layers of the MAO coatings have relatively a loose, porous and low hardness, the surfaces of the coatings are exposed to much less resistance against sliding.

The effect of the sodium silicate concentration on the coefficient of friction and surface roughness of the coatings are given in Fig. 9. As the sodium silicate concentration is increased, the coefficient of friction increases. This may be due to the changes in phase composition, hardness and a corresponding increase in a coarse-grained structure leading to high surface roughness. High surface roughness and granular and irregular coating products on the surface creates a resistance against sliding and cause an increase in the coefficient of friction.

Along with the images obtained from SEM, 3D (three-dimensional) wear tracks were also studied using a surface profilometer. The 3D profiles of the wear tracks developed on the surfaces of the as-deposited oxide coatings produced in different solutions during reciprocating wear tests are given in Fig. 10. As it is seen from the 3D profiles of the wear tracks, increasing sodium silicate concentration in the electrolyte increases the dept of wear track of the coating. The coating produced in E_1 solution is only composed of γ-Al_2O_3 and α-Al_2O_3 phases, while the coatings produced in E_2 and E_3 solutions are composed of γ-Al_2O_3, α-Al_2O_3 and mullite ($3Al_2O_3{\cdot}2SiO_2$) phases. The hardness of the coating consisting of γ-Al_2O_3 phase is higher than the one consisting of mullite. Increasing the sodium silicate concentration in the solution leads to decrease the hardness of the outer layer while it increases the thickness and porosity of the loose outer layer of the coatings. For this reason, the depth of wear track of the coating produced in solution E_1 is less than those produced in the other solutions. Due to

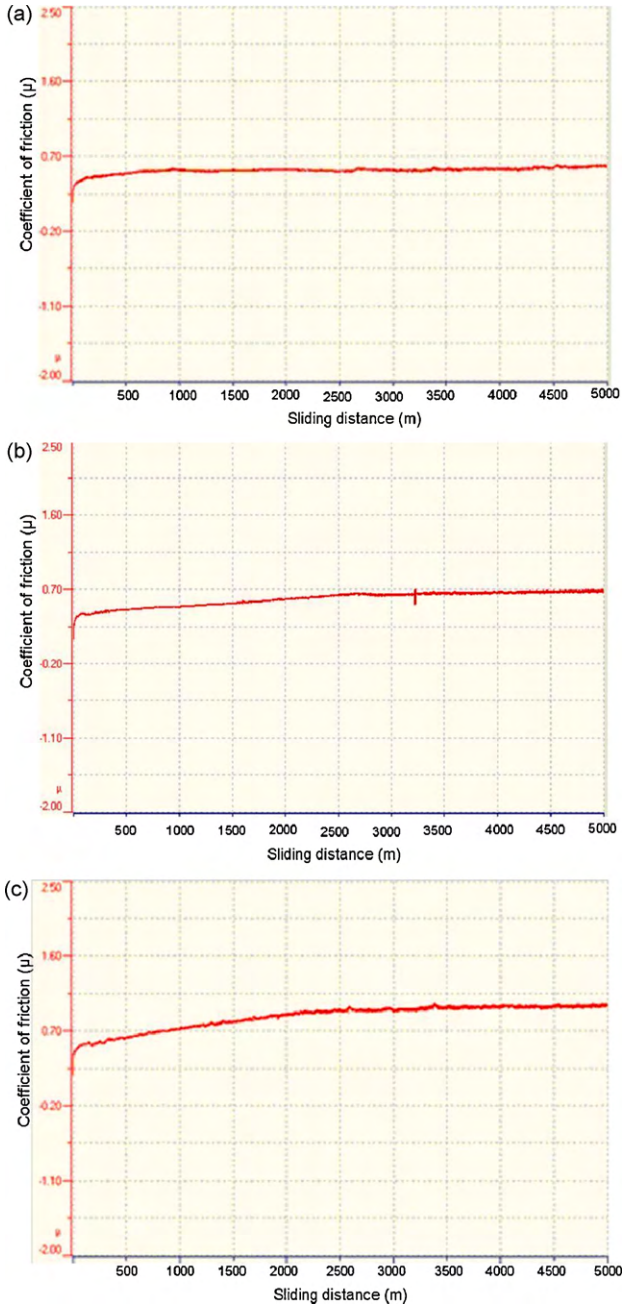

Fig. 8. Friction coefficient vs. sliding distance for the coating produced in different solutions: (a) solution E_1; (b) solution E_2; (c) solution E_3.

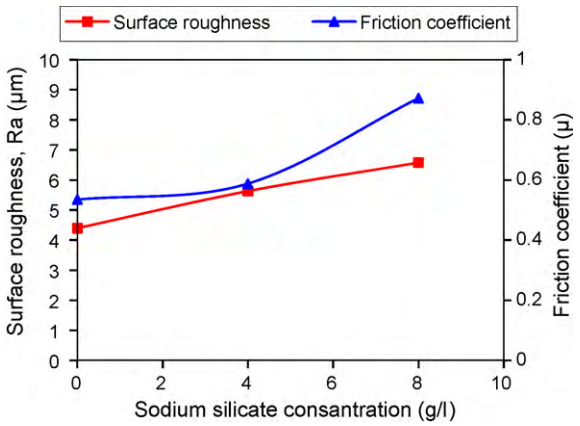

Fig. 9. Variations in the surface roughness and friction coefficient with the sodium silicate concentration.

wear, there is a change in the depth of wear track of the coating which is given in Table 2.

Considering the depth of wear tracks of the as-deposited oxide coatings, it was understood that almost no wear occurred in the inner layers of the coatings. The wear only occurred on the porous outer surface of the coatings. Therefore, it was identified that the results of wear represent only wear of the outer layer of the coatings. Since the inner region of the coatings is denser and harder than the outer part of the coating, it is expected that this regions would be more resistant to wear and its wear rate would be much lower. To verify this, the coatings produced in the different solutions were grounded (polished) from surface to interface of coating/substrate until a coating layer with 30 μm thickness remained on the surface of each coating and were subjected to wear test at the same test parameters. The related wear test results are also given in Table 2.

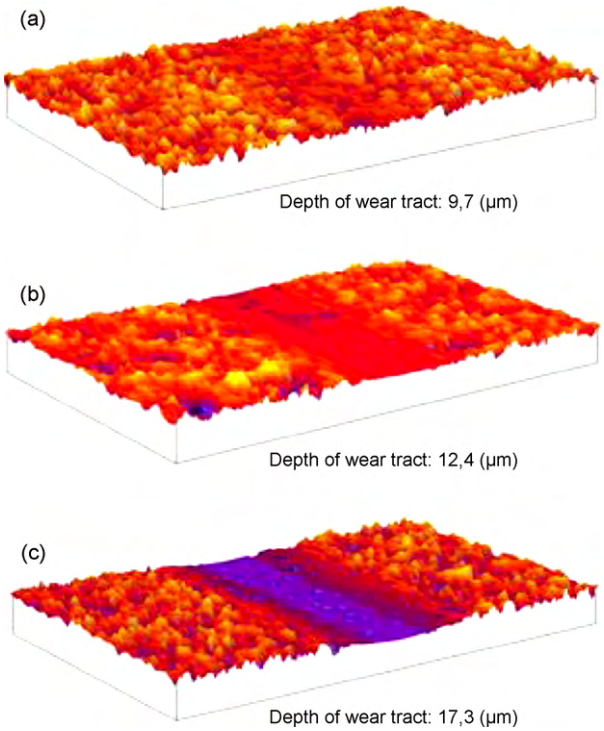

Fig. 10. 3D profiles of the wear tracks developed on the surfaces of the as-deposited oxide coating produced in different solutions: (a) solution E_1; (b) solution E_2; (c) solution E_3.

Table 3
Scratch test critical loads on the coating produced different solutions.

Solution	Coating thickness (μm)	Critical load L_c (N)
E_1	74	127.76
E_2	94	188.64
E_3	144	198.54

The coefficient of friction and the wear track depths obtained from the wear tests of the coatings grounded in this manner are lower than those of the as-deposited oxide coatings. The low coefficient of friction might be due to two reasons. One is the grounding of the surfaces of the coatings with a proper operation removes the extremely rough surface of the as-deposited oxide coating and makes surface smooth and generate a low friction with a low shear force. The other is that the very fine wear products produced during sliding enter into the micro pores present in the coating and partly act as a solid lubricant.

The low depth of wear track in the inner layer of the coatings is connected with a structural change in the coating's inner region. The inner layer was more compact than outer layer, and pore density decreased from outer layer to inner layer in MAO coatings (see Fig. 2). Comparing the depths of wear track of the each polished coatings (grounded to a thickness of 30 μm) produced in different solutions, it can be seen that the depth of wear track of the coating produced in E_2 solution is minimum, while the one of the coating produced in E_1 solution is maximum. The reason of this is that the surface of the polished coating produced in E_1 solution consists of high content of γ-Al_2O_3 phase with low density and low hardness, and low content of α-Al_2O_3 phase, while the one produced in E_2 solution consists of high content of α-Al_2O_3 phase with high density and high hardness.

3.7. Adhesion of the coating

The adhesion of coatings produced from different solution was investigated with a scratch test. The related scratch test results for the surface layer produced on 2017A alloy are given in Table 3. The critical load (L_c) at which adhesive failure of the coating occurred was detected by optical microscopic examination of the scratch track after the test. These measured critical loads are the characteristic values of each coating. The higher critical load, the better adhesion properties of the coating is achieved. The value of L_c increases with increasing sodium silicate concentration. The highest critical load was recorded for the coating produced in the E_3 solution whereas the coating produced in the E_1 showed the lowest one. The critical load value of the coating produced in E_3 solution is higher than the others. This could be explained by high hardness, high thickness, high load carrying capacity of coating and the way of connection of the interfacial region to substrate. Each coating with different hardness due to its coating thicknesses and phase structure has different load carrying capacity and causes different degree of plastic deformation on the substrate at the same amount of applied load.

An increase in the adhesion strength of MAO coating with increasing the coating thickness may be explained by MAO coating formation mechanism on aluminum alloys. With increasing the coating thickness, a larger volume of metal enters into the oxidation process and the adhesion strength of the coating increases even more. The metallurgical intermixing and inter diffusional bonding generated by microarc process also lead to high degree of interfacial adhesion between ceramic coatings and substrate [5]. In addition, coating produced by MAO method, in contrast to many other coating methods, grows into the substrate [6] and does not contain an artificial interface which would weaken the coating adhesion.

4. Conclusions

1. Increasing the sodium silicate concentration in the electrolyte leads to increase both the thickness of the dense and porous outer layer of the coatings, simultaneously. The increase in the thickness of the outer layer of the coatings is higher than the ones in the dense layer of the coatings.
2. The coating produced in the electrolyte with low sodium silicate concentration has higher microhardness values and better wear resistance than the one formed in the electrolyte with high sodium silicate concentration and in the electrolyte without sodium silicate. These increased hardness and wear resistance are the result of decreased coating porosity and increased ratio of coating with phase structure especially increased rate of α-Al_2O_3.
3. The introduction of sodium silicate into the electrolyte leads to significant change in the discharge characteristics of the sparks at the surface. High sodium silicate leads to increased sparking discharge intensity and contributes the accumulation of the coating products and forms a coarse-grained structure leading to a high surface roughness. The low sodium silicate tends to form fine grain structure and causes lower surface roughness contrarily to high sodium silicate.
4. Increasing the sodium silicate concentration in the electrolyte leads to increase both the thickness of coatings and adhesion strength of the coatings, simultaneously. An increase in the adhesion strength of MAO coating with increasing coating thickness may be explained by MAO coating formation mechanism on aluminum alloys.
5. The coatings produced in each of three different electrolytic solutions provide a high surface hardness, a good interfacial adhesion, a load carrying capacity and an excellent wear resistance to uncoated aluminum alloy.

References

[1] X. Nie, E.I. Meletis, J.C. Jianng, A. Leyland, A.L. Yerohkin, S.C. Jianga, A. Mattews, Surf. Coat. Technol. 149 (2002) 245–251.
[2] O. Fuchs, C. Friedrich, G. Berg, E. Broszeit, A. Leyland, A. Matthews, Mat.-wiss. u, Werkstofftech. 29 (1998) 141–152.
[3] S.H. Awad, H.C. Qian, Wear 260 (2006) 215–222.
[4] O. Wanstrand, M. Larsson, A. Kassman-Rudolphi, Surf. Coat. Technol. 127 (2000) 107–113.
[5] X. Nie, A. Leyland, H.W. Song, A.L. Yerohkin, S.J. Dowey, A. Mattews, Surf. Coat. Technol. 116–119 (1999) 1055–1060.
[6] W. Xue, Z. Deng, R. Chen, T. Zhang, Thin Solid Films 372 (2000) 114–117.
[7] A.L. Yerokhin, V.V. Lyubimov, R.V. Ashitkov, Ceram. Inter. 24 (1998) 1–6.
[8] G.L. Yang, X.Y. Lu, Y.Zh. Bai, H.F. Cui, Z.S. Jin, J. Alloys Compd. 345 (2002) 196–200.
[9] A.L. Yerokhin, X. Nie, A. Leyland, A. Matthews, S.J. Dowey, Surf. Coat. Technol. 122 (1999) 73–93.
[10] A.L. Yerokhin, X. Nie, A. Leyland, A. Matthews, Surf. Coat. Technol. 130 (2000) 195–206.
[11] X. Nie, A. Leyland, A.L. Yerokhin, H.W. Song, A. Matthews, Surf. Coat. Technol. 119 (1999) 1055–1060.
[12] G. Sandararajan, L. Rama Krishna, Surf. Coat. Technol. 167 (2003) 269–277.
[13] B.Y. Long, H.H. Wu, B.H. Long, J. Wang, J. Jilin Univ. 43 (2005) 68–72.
[14] H.H. Wu, X.Y. Lu, B.H. Long, X.Q. Wang, Mater. Lett. 59 (2005) 370–375.
[15] H.H. Wu, Z.S. Jin, B.Y. Long, F.R. Yu, X.Y. Lu, Chin. Phys. Lett. 20 (2003) 1815–1818.
[16] W. Krysman, P. Kurze, H.G. Dittrich, Crystal. Res. Technol. 19 (1984) 973–979.
[17] A. Polat, M. Usta, M. Makaracı, A. Ata, Z. Tas, Practical Metall. 45 (2008) 594–609.
[18] V.V. Bakovets, O.V. Polyakov, I.P. Dolgovesova, The Second International Symposium, Nauka, Novosibirsk, 1992, pp. 168–172.
[19] V.N. Malyshev, G.A. Markov, V.A. Fyodorov, A.A. Petrosyants, O.P. Terleeva, Khimicheskoye i Neftyanoye Mashinostroenije 1 (1984) 26–30.
[20] V.I. Tchernenko, L.A. Snezhko, S.B. Tchernova, Zashchita Met-allov. 18 (3) (1982) 454–458.
[21] G.A. Markov, B.S. Gizatullin, I.B. Rychazhkova, USSR Patent 926 083 (1982).
[22] S.V. Gnedenkov, P.S. Gordienko, S.L. Sinebryukhov, A.N. Kovryanov, O.A. Khrisanfova, A.I. Cherednichenko, S.V. Korkosh, Russ. J. Appl. Chem. 73 (2000) 6–9.
[23] G.A. Lavrushin, S.V. Gnedenkov, P.S. Gordienko, S.L. Sinebryukhov, Russ. Prot. Met. 38 (2002) 363–365.
[24] A.L. Yerokhin, X. Nie, A. Leyland, A. Matthews, Surf. Coat Technol. 130 (2000) 195–206.
[25] A.L. Yerokhin, L.O. Snizhko, N.L. Gurevina, A. Leyland, A.A. Pilkington, A. Matthews, Surf. Coat. Technol. 177 (2004) 779–783.
[26] W.B. Xue, C. Wang, R.Y. Chen, T.H. Zhang, Mater. Lett. 52 (2002) 435–441.
[27] W.B. Xue, Z.W. Deng, H. Ma, R.Y. Chen, Surf. Eng. 17 (2001) 323–326.
[28] V.S. Rudnev, L.M. Tyrina, V.M. Nikitin, N.V. Speshneva, P.S. Gordienko, Russ. Prot. Met. 39 (2003) 334–337.
[29] J. Tian, Z. Luo, S. Qi, X. Sun, Surf. Coat. Technnol. 154 (2002) 1–7.
[30] Y. Han, S.H. Hong, K.W. Xu, Surf. Coat. Technol. 154 (2002) 314–318.
[31] J.P. Schreckenbach, G. Marx, F. Schlottig, M. Textor, N.D. Spencer, J. Mater. Sci. Mater. 10 (1999) 453–457.
[32] S.V. Gnedenkov, P.S. Gordienko, O.A. Khrisanfova, T.M. Scorobogatova, S.L. Sinebrukhov, J. Mater. Sci. 37 (2002) 2263–2265.
[33] P.S. Gordienko, S.V. Gnedenkov, S.L. Sinebryukhov, O.A. Khrisanfova, T.M. Skorobogatova, Russ. Electrochem. 29 (1993) 1232–1238.
[34] C. Wang, D. Zhang, Y. Jiang, Appl. Surf. Sci. 253 (2006) 654–670.
[35] W. Xue, C. Wang, Y. Li, R. Chen, T. Zhang, ISIJ Int. 42 (2002) 1273–1277.
[36] S.J. Bull, D.S. Rickerby, A. Matthews, A. Leyland, A.R. Pace, J. Valli, Surf. Coat. Technol. 36 (1988) 503–517.